Investigation of Al-Ti Nano Graphene Hybrid Approach in Power Mixed EDM: Advancing Electrical Conductivity, Stability, and Material Removal with Ceramic Integration

Hassan Karim Mohammed[1], Jamaluddin Abdullah[1*], Muhammad Hafiz Bin Hassan[1], Salah S. Abed AlKareem[2]

[1]*School of Mechanical Engineering, University Sains Malaysia, Malaysia.*
[2]*Department of Automated Manufacturing Engineering, Al-Khwarizmi College of Engineering, University of Baghdad, Iraq*
Email: mejamal@usm.my

Abstract: The composite Al-Ti nano graphene alloy is efficient for industrial applications. Few research created nano graphene-aluminum composites. This research uses electrical arc machining to examine the effects of Al-Ti nano graphene composites on hardness, removal rate, roughness, resistance, and microstructure. The MIKROTOOLS DT- 110, with micromachining and high accuracy, was used for this work. Olympus SZX-12, Zeiss Supra 35 VP scanning electron microscope, and Energy Dispersive Spectroscopy were utilized to evaluate novel Al-Ti nano composites. Micro EDM, powder mixed micro-EDM, and die-sinker EDM were the major experimental methods. This study found steady improvement in corrected electrical conductivity, optimized machinery efficiency, Kojima and Pandey plasma channel radius approximations, and maximum heat flux approximations for the formulated new aluminum composites. The present study found successful machining with low material removal rate; cardon deposition controlled machining outputs (surface cracks and porosity); hybrid process achieved successful machining and removal rate; and high performance properties for the developed composites compared to conventional types. This research found the hybrid Al-Ti nano graphene method important for electric conductivity, stability, and material removal. This is the first research to examine power mixed EDM's advantages from ceramics with optimum performance.

Keywords: Hybrid Al-Ti Nano Graphene, Power Mixed EDM, Ceramic Integration, Electrical Conductivity.

1. Introduction

Lightweight materials save fuel and reduce carbon emissions. Aluminum and titanium alloys are employed in many sectors owing to their low bulk density and high strength-to- weight ratio. However, its limited ductility and wear resistance restrict its use. Nanoscale reinforcements like graphene were added to Al-Ti alloys to build composite materials to overcome these restrictions.

Composite Al-Ti-nano graphene alloys offer several advantages over standard alloys, but their low strength and ductility make them hard to process. Electrical arc machining can shape and machine these materials. Arc machining for Al-Ti nanographene composite alloys was tested

to determine how process parameters effect material removal rate, surface roughness, and product microstructure. To determine electrical arc machining capability on Al-Ti-nano graphene alloys. This study may enhance lightweight material machining and production processes.

The strength-to-weight ratio of titanium and its alloys is outstanding even at high temperatures. These metals are valuable in medical, aerospace, nautical, chemical, and food industries due to their corrosion and erosion resistance. Their biocompatibility makes them popular in implanted medical technology. Military vehicles are protected by Ti6Al4V alloy's ballistic performance. Non-ferromagnetic titanium implants may be analyzed using MRI and NMRT. Titanium's limited thermal conductivity concentrates heat at the tool/chip contact, causing substantial working zone temperature variations. Thus, tools wear quicker and shatter. Hot and chemically reactive titanium may fuse the tool into the metal and shatter it. Titanium's low modulus causes component bending, clatter, and vibration in machining. Given these constraints in typical titanium processing, non-traditional methodologies are needed to study titanium machinability. Wire electrical discharge machining is one method.

WEDM (wire EDM) works best with materials with strong mechanical qualities and high electrical conductivity. Wire Erosion Machining (WEDM) removes material by discharging a current over a narrow electrode gap using pulsing DC power. Thin and robust, the cutting wire makes clean, precise cuts.

Optimizing process parameters is crucial for green manufacturing. Several scientists determined the best WEDM settings for milling Ti6Al4V. Any experiment requires meticulous planning to save time, money, resources, etc. RSM, Taguchi with orthogonal arrays, and partial factorial designs are experiment designs. Trial findings are utilized to fine-tune input process parameters. Multiple replies must be optimized in modern manufacturing. GRA, HTS, supervised learning-based, and particle swarm algorithms may be utilized to develop a step-off solution for optimal process parameters. Many studies have examined genetic algorithms, artificial neural networks, etc.

Many extreme engineering applications need high-performance materials. Al-Ti-nano graphene alloy materials need additional property improvement, which hinders their applicability. Improving material hardness and wear and chemical resistance is crucial. The Al-Ti-nano graphene alloy can tolerate temperatures above superalloys (Farooqui & Patil, 2018). They might be used in extreme heat. This may increase gas turbine power, temperature, and efficiency (Rajeevalochanam & Ganesh Banda, 2017). Industrial applications for enhanced Al-Ti-nano graphene alloy are possible (Dhir, Ghataora & Lynn, 2017). Multidisciplinary researchers are studying these materials' machining. Brittleness and cutting pressures prevent conventional machining of Al-Ti-nano graphene alloy. Some non- conventional techniques can manufacture Al-Ti-nano graphene alloy. The issue of getting an accurate form without microcracks remains (Zheng et al., 2019). Microcracks are difficult to avoid even with sophisticated laser beam and electric beam machining (Xing et al., 2018). Electric Arc Machining (EAM) is a practical non-conventional machining technology for electrically conductive, hard-to-cut materials. EAM can form wear-resistant materials into complicated shapes (Uhlmann & Domingos, 2016; 2013; Kumar et al., 2018). EAM may create bores, grooves, and undercuts in tiny hard components (Gupta & Jain, 2014; Chen et al., 2018).

EAM is a non-contact process that can machine insulators like alloy materials and semiconductors, but it requires an electrically conductive workpiece. Recent experiments have shown that it can do so. The heat resistance of advanced alloys like Al-Ti-nano graphene alloy makes them popular in transport, energy, semiconductor, and healthcare applications (Teo, 1999). Using EAM to machine insulating ceramics would allow Al-Ti-nano graphene alloy to be used in numerous creative and complex industrial applications. EAM's helping electrode approach has been used to process insulating ceramics via material removal for years. This mechanism is unstable when the conductive layer is depleted (Mohri, 1996). Other researchers

have conducted few insulating alloy trials. This work aims to alter the fundamental assistive electrode technology to manufacture insulating Al-Ti-nano graphene alloy materials sustainably. This research effort focuses on EAM of Al-Ti-nano graphene alloy, an insulating alloy used in numerous engineering fields.

2. Methodology

This study was carried out in Northern Iraq's control Public Laboratory. This study seeks an EAM approach to manufacture Al-Ti-nano graphene alloys. Since Al-Ti-nano graphene alloy is insulating, it was selected for this project. All tests were done on AIN ceramics. Only under precise machining settings has electrode material or powder particles transferred from dielectric to work surface. Thus, surface modification procedure parameters must be chosen carefully. Surface quality and topography rely on process parameter and P/M electrode parameter.

2.1 Technical Specifications for Machine Tools

Experiments were conducted on two EDM machines: a MIKROTOOLS DT-110 for micro-EDM and an EXCETEK ED 400 for die-sinker EDM.

1- MIKROTOOLS DT-110 (Micro-EDM Machine): This high-precision, multi- process apparatus was used for preliminary micro-machining. The capacity to manufacture electrodes directly on the apparatus reduced errors. The specifications are shown in Table 1.

Table 1. Specifications of EDM machine

Machine Element	Specification
Monolithic natural granite base	
Size of Oil Container:	650 X 400 X 300 mm
Table Size:	400 X 250 mm
X-Axis travel:	250 mm
Y-Axis travel:	150 mm
Z-Axis travel:	150 mm
Maximum job height:	165 mm
Maximum job weight:	150 kg
Maximum current:	25 Amp
Best MMR:	140 mm3
Connected load:	2 KVA
die electric tank capacity:	200 ltr
Supply Volts:	415 V, 3 Ø, 50 Hz
Maximum Table-Quill distance:	340 mm
Minimum Table-Quill distance:	190 mm
Vibration Isolation	4-point heavy duty passive dampers
AC servo motor	100 W (1 to 5000 rpm)
Without tool change function	20000 rpm or 60000 rpm
With tool change function	6000 rpm Accuracy:
Resolution	100nm
Accuracy	+/-100mm
Repeatability	1 micron for all axes

2- EXCETEK ED 400 (Die-Sinker EDM): Employed for machining bigger features subsequent to successful micro-EDM trials. The specifications are defined in Table 2.

Table 2. Specifications of EXCETEK ED 400

Criteria	Description
C codes	Predefined 2000 sets
Pulse-on time	0-2000 μs
Pulse-off time	0-4000 μs
Peak current	0-288 amps
HV discharge	140V-235V DC
LV discharge	0.4-1.8 amps
Discharge time	0.1s-99.9s
Gap voltage	20-120 V
Swing radius	0-999 mm
Electrode polarity	Reversible
Discharge server speed	Controllable
Slag removing speed	Controllable

2.2 Workpiece material

The workpiece material used was an Al-Ti-nano graphene hybrid alloy. The composition and characteristics of the alloy are shown in Table 3. The integration of ceramics was accomplished by using aluminum nitride (AIN) as the insulating medium. Workpieces were fabricated by cutting and polishing the alloy to specified dimensions (40 mm × 40 mm × 1.4 mm). The samples were further machined using micro-EDM and die-sinker EDM techniques under diverse circumstances, focusing on surface integrity and material removal rate (MRR).

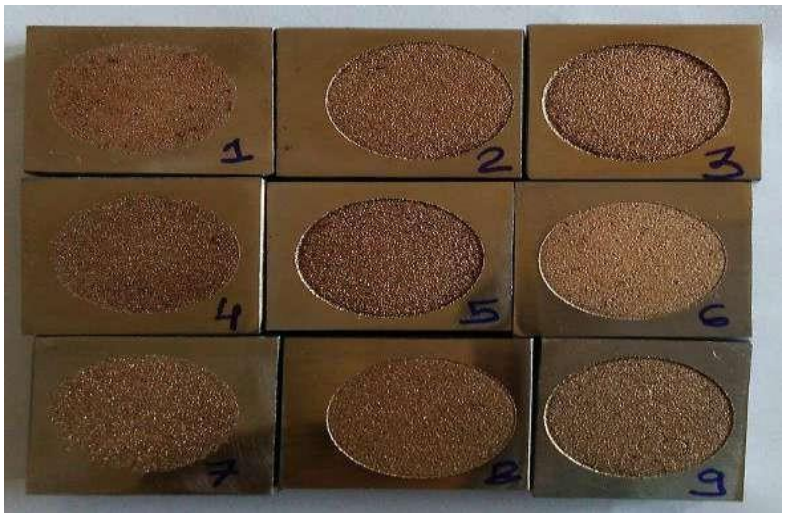

Figure 1: Machined Samples of Workpieces

Table 3. Properties of MMCs with Metals

Properties	Aluminum/SiC	Aluminium/Graphite	Steel	Aluminium
Ultimate Tensile Strength (MPa)	1206	448.2	648.1	234.4
Coefficient of thermal expansion (μm/m/^{0}C	12.4	18	11.7	23
Young's Modulus (GPa)	117.2	124.1	206.8	68.95
Specific Gravity	2.6	2.2	7.8	2.6

2.3 Preparation of Electrodes by Powder Metallurgy

The electrodes were comprised of copper, tungsten, and silicon powders blended in specified proportions (Cu 75%, W 23%, Si 2%). The electrodes for powder metallurgy (P/M) were fabricated by the following procedures:

1- Weighing and Mixing: Fine metallic powders were measured and combined using a custom-designed stirrer.

2- Compaction: The blended particles were compressed with a hydraulic press under regulated pressure. The procedure yielded diminutive electrodes that were secured for EDM operations.

2.4 Experimental Configuration and Methodology

2.4.1 Traditional Micro-Electrical Discharge Machining

The first round of tests used the aided electrode technique, using a conductive layer on the ceramic surface. This technique facilitated the deposition of conductive material during machining, preserving the EDM process even with non-conductive ceramics Figure 3. The material removal rate (MRR) was assessed by optical microscope techniques.

2.4.2 Powder-Mixed Micro-Electrical Discharge Machining

A hybrid technique was subsequently used, including conductive particles (Cu, W, Si) into the dielectric fluid. This enhancement optimized the machining process by augmenting the material removal rate, decreasing machining duration, and improving surface smoothness. The influence of powder concentration, particle size, and dielectric composition was examined to enhance the process.

2.4.3 Die-Sinker Electrical Discharge Machining

Upon determining the ideal settings and methods using micro-EDM, the concluding tests were conducted on a larger scale utilizing die-sinker EDM. More substantial apertures were fabricated employing elevated current and voltage parameters, concentrating on optimizing material removal rate and reducing electrode degradation.

2.5 Analytical Methodologies

1- Optical Microscopy: An Olympus SZX-12 microscope was used to ascertain the size of the machined apertures and compute the Material Removal Rate (MRR).

2- Scanning Electron Microscopy (SEM): A Zeiss Supra 35 VP SEM was used to examine surface morphology, material deposition, and removal procedures at elevated magnifications.

3- Energy Dispersive Spectroscopy (EDS): EDS analysis was conducted to examine the elemental composition of the machined surfaces, yielding insights into material movement and deposition processes.

3. Results and Discussions

This study aimed to enhance the machinability of non-conductive ceramic materials using powder-mixed EDM. Various machining attempts and coating setups were tested to identify optimal conditions for successful machining. The key findings are structured around the factors influencing EDM process efficiency and material removal rates.

3.1 Evaluation of Coating Materials

A 700 µm machining depth hole was successfully machined using a 600 µm diameter tool in the first example. Figure 2(a) shows the SEM picture of the blind micro-hole machined in AIN ceramics with two silver coatings and silver nanoparticles on top. First, silver nanoparticles and coating were fused on the ceramic surface to be machined. For 60 minutes, a 900 °C sintering oven was used. A hand paintbrush applies the second coating of silver, which is sintered in an oven at 900 °C for 60 min. Here, copper tungsten electrode was employed. Magnified SEM images at the micro-hole edges demonstrate the double layer of

conductive coating, as illustrated in Figure 2(b). Machined depths are seen below the two conductive silver coats. The SEM picture shows a machined hole diameter of 759 µm, resulting in an 80 µm overcut for blind micro-holes. Figure 3a displays machined surface topography SEM images. Although the discharge energy employed for machining was low, the photos show rough cut surfaces. The no-tool rotation situation allowed removed material to rest on the hole bottom, causing this increased roughness. SEM picture shows that intergranular cracking causes thermal spalling of complete grains off the machined surface during EDM for this ceramic. Thus, thermal spalling and nitrogen gas-releasing ceramics remove this ceramic. The machined surfaces show melting and evaporation, not only thermal spalling. Several thermal fractures and porosity on the machined surface as shown in Figure 3 (a and b).

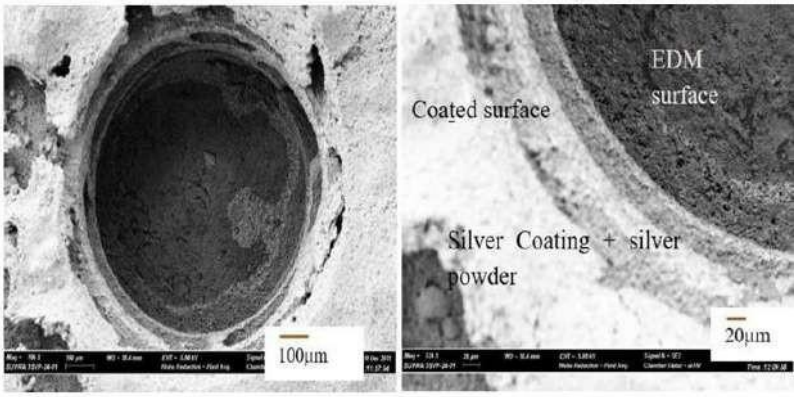

(a) (b)

Figures 2: (a) SEM image of a micro-hole machined on coated AlN ceramic surface; (b) SEM imageshowing the layers of silver coatings on AIN ceramic surface and the machined surface

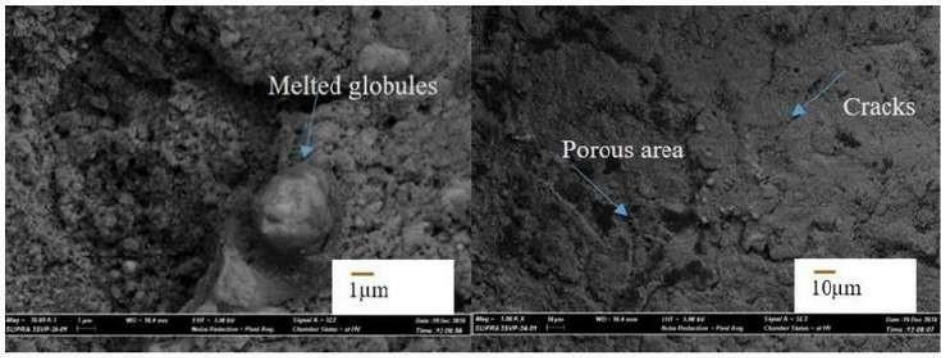

(a) (b)

Figures 3: SEM images of the machines surface at the bottom of the blind micro-hole. (a) meltedglobules on the surface; (b) thermal cracks and porosity on the surface

The coating layer and machining surface were compared using EDS spectral analysis on the top and bottom of the hole. EDS spectrum analysis of the machined surface from the micro- hole bottom is shown in Figure 4. The elemental composition shows aluminum and nitrogen on the machined surface. Surface copper and tungsten come from the tool electrode. The machined surface has a lot of oxygen. Carbon on the surface comes from dielectric breakdown. As seen in Figure 5, the EDS spectrum on the top surface of the machined hole (on the silver coating layers) shows silver, oxygen, carbon, and silicon on the coating layer, but no or little aluminum or nitrogen, the main ceramic constituents. The presence of aluminum and nitrogen on the machined surface was confirmed through EDS spectrum analysis (Figures 4,5), indicating that the machining extended beyond the conductive layer.

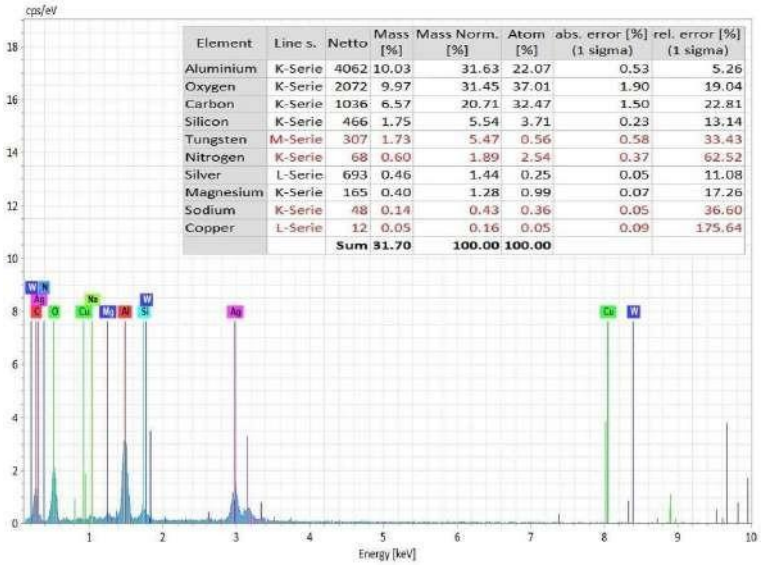

Element	Line s.	Netto	Mass [%]	Mass Norm. [%]	Atom [%]	abs. error [%] (1 sigma)	rel. error [%] (1 sigma)
Aluminium	K-Serie	4062	10.03	31.63	22.07	0.53	5.26
Oxygen	K-Serie	2072	9.97	31.45	37.01	1.90	19.04
Carbon	K-Serie	1036	6.57	20.71	32.47	1.50	22.81
Silicon	K-Serie	466	1.75	5.54	3.71	0.23	13.14
Tungsten	M-Serie	307	1.73	5.47	0.56	0.58	33.43
Nitrogen	K-Serie	68	0.60	1.89	2.54	0.37	62.52
Silver	L-Serie	693	0.46	1.44	0.25	0.05	11.08
Magnesium	K-Serie	165	0.40	1.28	0.99	0.07	17.26
Sodium	K-Serie	48	0.14	0.43	0.36	0.05	36.60
Copper	L-Serie	12	0.05	0.16	0.05	0.09	175.64
		Sum	31.70	100.00	100.00		

Figure 4: EDS Spectrum analysis on the machined surface (at the bottom of the micro-hole) with elemental composition analysis

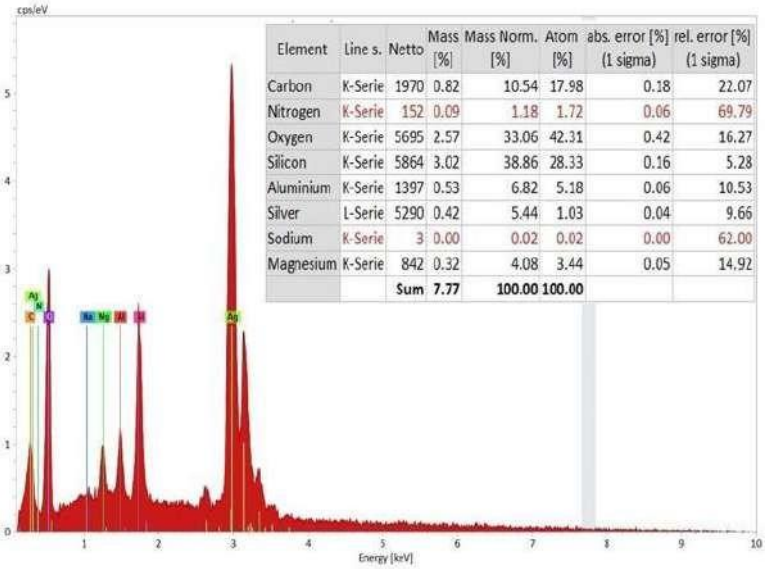

Element	Line s.	Netto	Mass [%]	Mass Norm. [%]	Atom [%]	abs. error [%] (1 sigma)	rel. error [%] (1 sigma)
Carbon	K-Serie	1970	0.82	10.54	17.98	0.18	22.07
Nitrogen	K-Serie	152	0.09	1.18	1.72	0.06	69.79
Oxygen	K-Serie	5695	2.57	33.06	42.31	0.42	16.27
Silicon	K-Serie	5864	3.02	38.86	28.33	0.16	5.28
Aluminium	K-Serie	1397	0.53	6.82	5.18	0.06	10.53
Silver	L-Serie	5290	0.42	5.44	1.03	0.04	9.66
Sodium	K-Serie	3	0.00	0.02	0.02	0.00	62.00
Magnesium	K-Serie	842	0.32	4.08	3.44	0.05	14.92
		Sum	7.77	100.00	100.00		

Figure 5: EDS Spectrum analysis on the coating layer (at the top and side of the micro-hole) with elemental composition analysis

Copper Tape Coating: Triple-layer copper tape also demonstrated some machining success, as seen in Case 2 (Table 4). The machined surface showed roughness and micro-cracks, but the process reached a depth of 700 µm. The presence of copper on the machined surface, as seen through EDS analysis (Figure 6.7), suggested deposition of conductive material from the tape.

Table 4. Successful Machining Attempts for Powder-Mixed Micro-EDM Process

Parameter	Case 1	Case 2	Case 3
Ceramic	AIN	AIN	AIN
Coating setup	Silver nanoparticles sandwiched between two layers of silver with copper on top, baked at 900º Celsius for 60 minutes	Silver nanoparticles sandwiched between two layers of silver with copper on top, baked at 900º Celsius for 60 minutes	Silver nanoparticles sandwiched between two layers of silver with copper on top, baked at 900º Celsius for 60 minutes
Tool	Copper-tungsten	Copper-tungsten	Copper-tungsten
Tool diameter	310 µm	310 µm	308 µm

Tool rotation	No rotation	No rotation	No rotation
Dielectric	Hydrocarbon oil	Hydrocarbon oil	Hydrocarbon oil
Powder material	Silver nanoparticle	Silver nanoparticle	Silver nanoparticle
Powder density	100 mg/L	100 mg/L	100 mg/L
Flushing condition	No flushing	No flushing	No flushing
Voltage	80 V	80 V	80 V
Capacitance	100 nF	1000 pF	100 nF
Depth of hole	996 µm	287 µm	1693 µm
Tool wear	0 µm	0 µm	244 µm

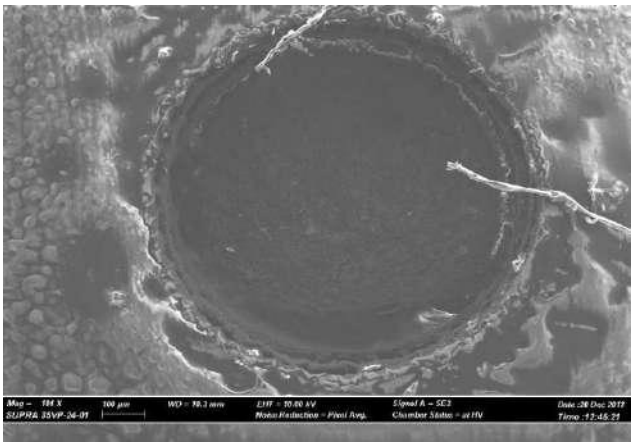

Figure 6: SEM image of the micro-hole on copper tape coated ceramic surface

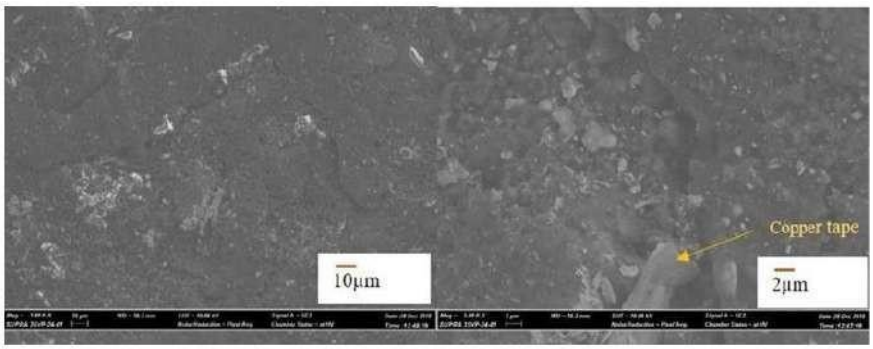

(a) (b)

Figure 7: SEM images of the machined surface at the bottom of micro-hole

3.2 Powder-Mixed EDM Approach

The introduction of silver nanoparticles into the dielectric significantly improved the machinability of ceramics in EDM, enhancing material removal rates and reducing machining times. The powder-mixed EDM process, combined with a three-layer conductive coating structure, achieved aspect ratios greater than 3 (Figures 8 and 9). The improved deposition of conductive powders during machining enhanced the EDM process's stability and material removal depth.

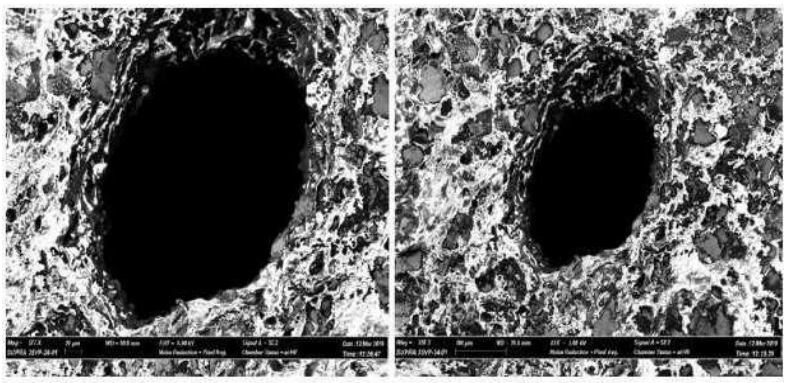

(a) (b)

Figure 8: Micro hole on the coated ceramic surface (Capacitance: 100 nF, Voltage: 80V), Case 1

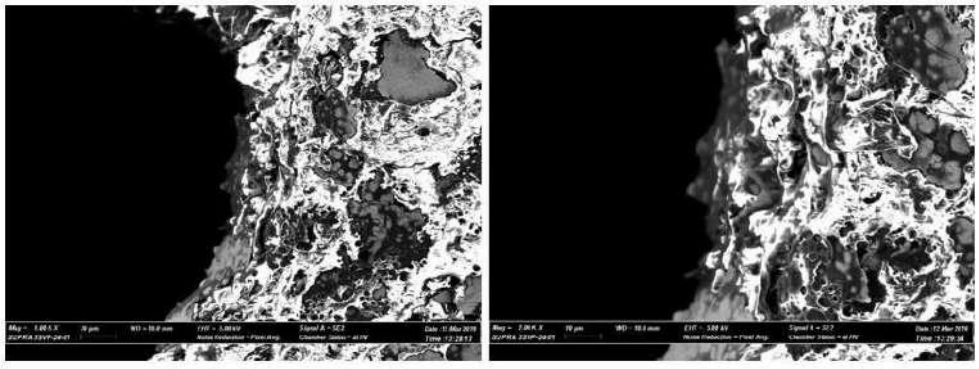

(a) (b)

Figure 9: Machined surface wall (Capacitance: 100 nF, Voltage: 80V), Case 1

3.3 Machining Improvement and Parameter Optimization

Optimal conditions for successful machining included:

1. Low voltage and capacitance for reduced energy sparks.
2. Stationary tools with no flushing, enabling stable carbon deposition on the machined surfaces, enhancing spark stability and reducing tool wear.
3. Longer machining times were required due to low energy sparks.

The machining quality and success were confirmed by analyzing the elemental composition of the machined surfaces, with clear signs of material removal extending beyond the conductive coating layers (Figures 10, 11).

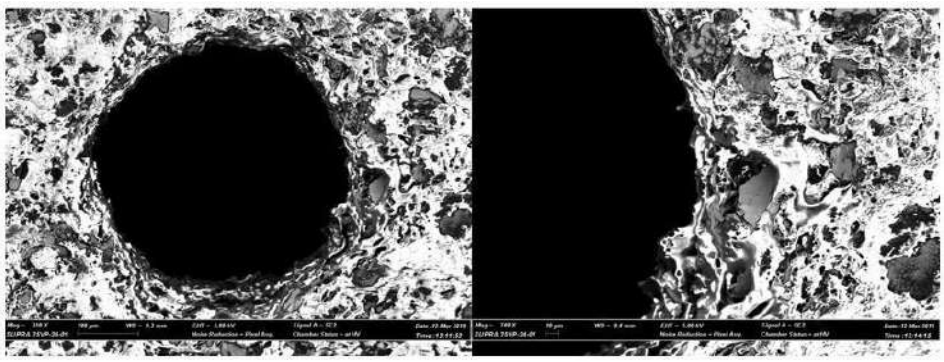

(a) (b)

Figure 10: (a) SEM image of a micro-hole machined on coated AlN ceramic, (b) side wall of the microhole surface for powder mixed EDM

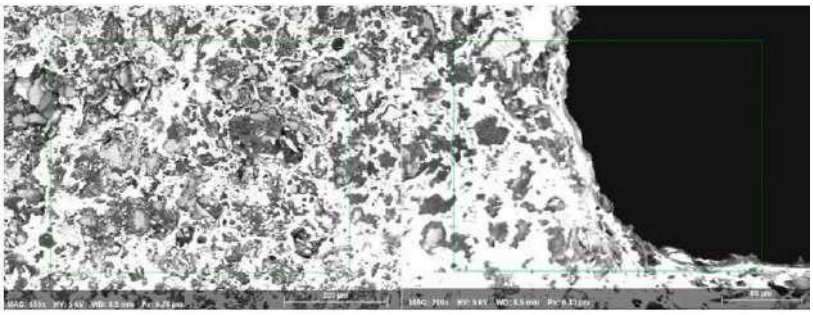

(a) (b)

Figure 11: EDS analysis has been taken from (a) un-machined coating surface and (b) edge of the micro-hole, obtained in AlN ceramic using combined assistive electrode and powder mixed EDM method

In case 3 of Table 4, the blind hole was too deep for the SEM to concentrate on, therefore EDS investigation at the bottom of the machined surface was impossible. EDS studies were done at three places surrounding and on the machined hole. Figure 12a shows EDS studies of the un-machined coating layer and micro-hole edge. In AlN ceramics, EDS spectrums were collected from both un-machined and machined surfaces of the micro-hole utilizing the assistive electrode approach and powder mixed EDM. EDS spectra elemental composition is presented in Figure 12b. Due to the coating layer, the un-machined surface has more silver and copper. The un- machined coating surface has practically little aluminum or nitrogen. The micro-hole edge has a different elemental makeup than the un-machined surface. The proportion of Al and N rose little, whereas C and W increased dramatically compared to the un- machined surface. The ceramic components at the micro-hole edge are shown by the modest Al and N percentage. While the higher C and W percentages imply material migration from the tool and disintegrated dielectric into the machined surface, or micro-hole edge.

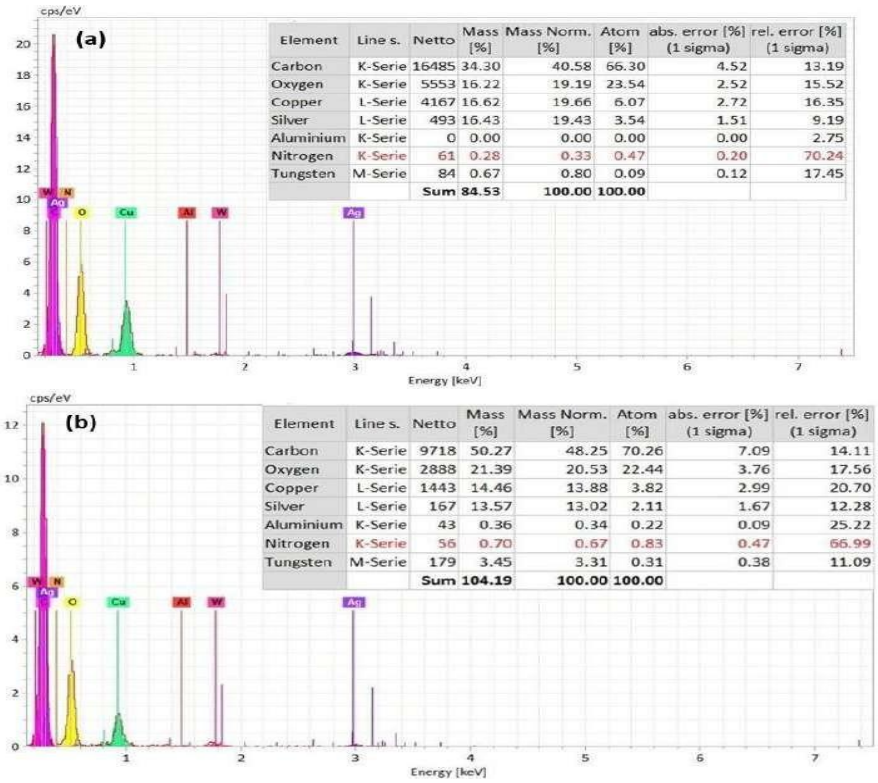

Element	Line s.	Netto	Mass [%]	Mass Norm. [%]	Atom [%]	abs. error [%] (1 sigma)	rel. error [%] (1 sigma)
Carbon	K-Serie	16485	34.30	40.58	66.30	4.52	13.19
Oxygen	K-Serie	5553	16.22	19.19	23.54	2.52	15.52
Copper	L-Serie	4167	16.62	19.66	6.07	2.72	16.35
Silver	L-Serie	493	16.43	19.43	3.54	1.51	9.19
Aluminium	K-Serie	0	0.00	0.00	0.00	0.00	2.75
Nitrogen	K-Serie	61	0.28	0.33	0.47	0.20	70.24
Tungsten	M-Serie	84	0.67	0.80	0.09	0.12	17.45
		Sum	84.53	100.00	100.00		

Element	Line s.	Netto	Mass [%]	Mass Norm. [%]	Atom [%]	abs. error [%] (1 sigma)	rel. error [%] (1 sigma)
Carbon	K-Serie	9718	50.27	48.25	70.26	7.09	14.11
Oxygen	K-Serie	2888	21.39	20.53	22.44	3.76	17.56
Copper	L-Serie	1443	14.46	13.88	3.82	2.99	20.70
Silver	L-Serie	167	13.57	13.02	2.11	1.67	12.28
Aluminium	K-Serie	43	0.36	0.34	0.22	0.09	25.22
Nitrogen	K-Serie	56	0.70	0.67	0.83	0.47	66.99
Tungsten	M-Serie	179	3.45	3.31	0.31	0.38	11.09
		Sum	104.19	100.00	100.00		

Figure 12: EDS spectrums with elemental composition taken from different spots of the micro-hole machined on AlN ceramic using assisted electrode method with powder mixed EDM; (a) un- machinedcoating surface and (b) edge of the micro-hole

3.4 Quality of Machined Holes

The die-sinker EDM approach produced well-defined through-holes in AlN ceramics, with rough surface textures evident from SEM images. The entrance of the holes had higher radial overcut, while the exit was more dimensionally accurate. The machining time and material removal rates were documented in Table 5 and depicted graphically in Figures 13,14.

Table 5. Dimensions and Machining Time of Machined Holes

Hole number	Avg Entrance diameter (mm)	Avg Exit diameter (mm)
Hole 1	3.93	2.89
Hole 2	4.04	2.26
Hole 3	4.36	2.68
Hole 4	4.65	2.42
Hole 5	4.65	2.63

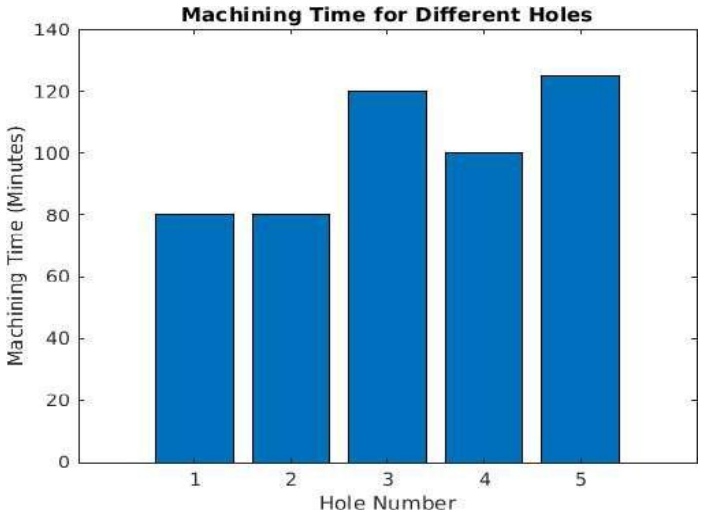

Figure 13: Machining time for different through holes; (a) Hole 1: Ip 1A, Ton 100 µs, Toff 200 µs (b) Hole 2: Ip 1A, Ton 100 µs, Toff 300 µs (c) Hole 3: Ip 1A, Ton 200 µs, Toff 300 µs (d) Hole 4: Ip 1A, Ton 200µs, Toff 400 µs (e) Hole 5: Ip 1A, Ton 300 µs, Toff 600 µs

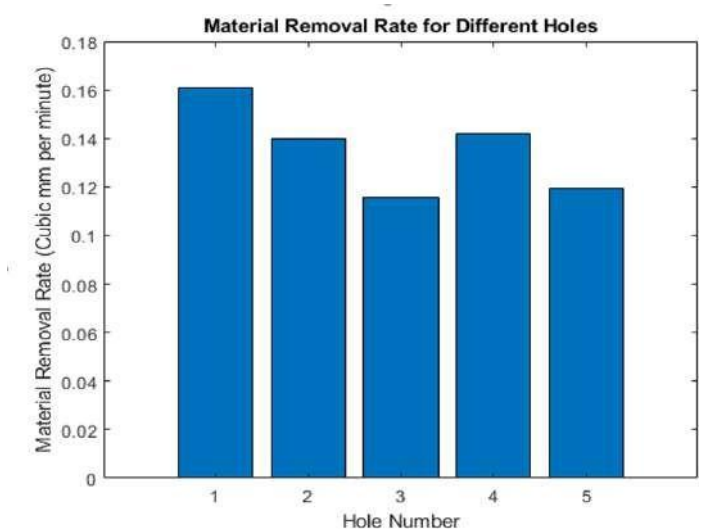

Figure 14: Material removal rate for different through holes; (a) Hole 1: Ip 1A, Ton 100 µs, Toff 200 µs (b) Hole 2: Ip 1A, Ton 100 µs, Toff 300 µs (c) Hole 3: Ip 1A, Ton 200 µs, Toff 300 µs (d) Hole 4: Ip 1A, Ton 200 µs, Toff 400 µs (e) Hole 5: Ip 1A, Ton 300 µs, Toff 600 µs

Figure 15 shows optical microscope images of hole entrances and exits. The machined surface's rough walls. This method's rough machined surface is constant across all parameters. The holes'

entrances and exits are readily visible. Copper tape on the workpiece sides resolidified during milling. Surface cylindricity is unclear. Hole entrances have greater radial overcut. Sparks should be stronger and more frequent while cutting the conductive layer. This increases radial overcut. Since sparks only occur in carbon-deposited regions, spark intensity should decrease as machining continues toward the ceramic area. Thus, inside ceramic, hole circularity improves and exit is more exact than entry.

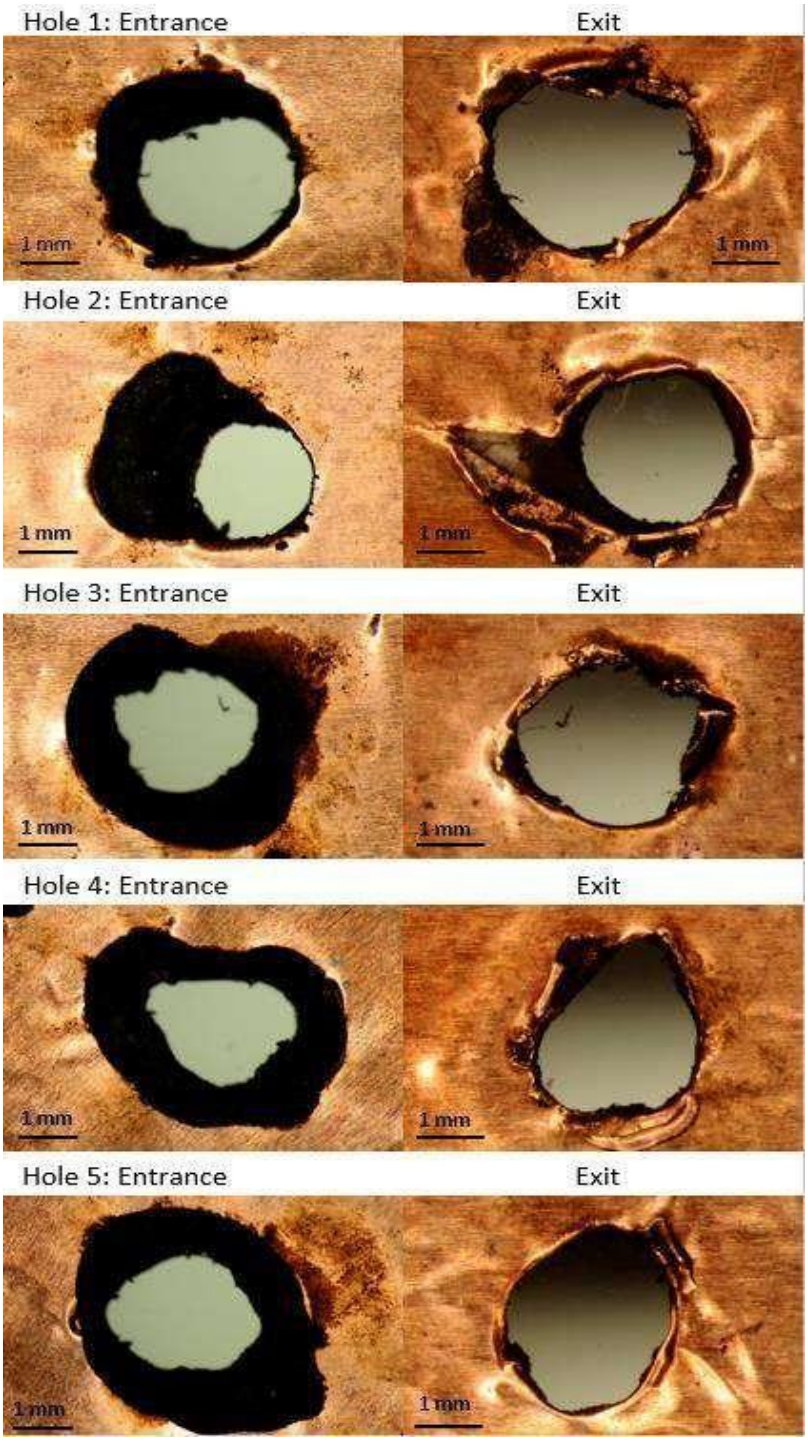

Figure 15: Entrance and Exit side of holes drilled (a) Hole 1: Ip 1A, Ton 100 µs, Toff 200 µs (b) Hole 2: Ip 1A, Ton 100 µs, Toff 300 µs (c) Hole 3: Ip 1A, Ton 200 µs, Toff 300 µs (d) Hole 4: Ip 1A, Ton 200 µs, Toff 400 µs (e) Hole 5: Ip 1A, Ton 300 µs, Toff 600 µs

This process deposits more carbon than prior methods. As indicated, aided electrode EDM machinability depends on carbon deposition. Figure 16 compares the average carbon deposition for this thesis's techniques. Carbon deposition enhanced powder mixed EDM machinability from the feasibility study. Compared to powder mixed EDM, the sandwich structure's machined wall has roughly twice as much carbon deposition. This research accomplished its aim of optimizing coating carbon deposition. Increased carbon deposition enhances machining depth and allows AIN ceramic through hole machining.

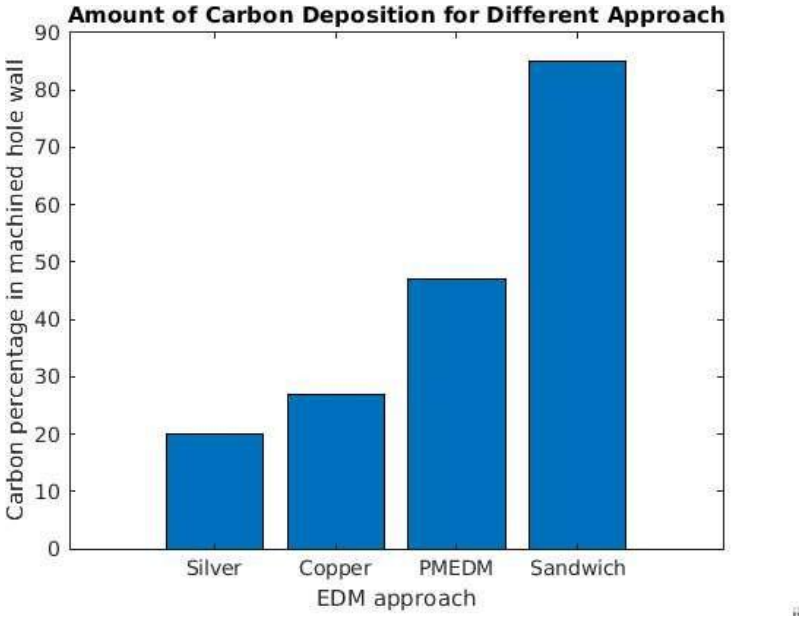

Figure 16: Amount of carbon deposition for different approaches

The amount of heat flux generated is an important parameter to understand the EDM process. AsEDM works by melting the workpiece in most of the cases, heat flux can be a determining factor to understand the material removal mechanism. Heat flux is usually highest in the proximity of the electrode. The maximum heat flux can be found on the surface of the electrode and near the machining zone. The heat flux is maximum in the region near the electrode and then reduces in a cylindrical coordinate with radius measure from the electrode. The amount of heat flux decreases radially with distance from the electrode surface. So, the region of maximum heat flux is actually working towards material removal. The maximum heat flux generated in EDM process can be approximated through empirical formulas Joshi et al. (2010)

$$Q_{max} = \frac{4.57 F_c V I}{\pi r_{p\_m}^2}$$

Q_{max}: Maximum heat flux in W/m^2
V: applied voltage, 80V as per experiments I: peak current, 1A as per experiments
r_{p_m}: plasma channel radius in meter
F_C: energy fraction to cathode, taken to be 0.183 according to literature

Figure 8 shows that plasma channel radius determines maximal heat flow. Machined high conductivity materials have a different plasma channel radius than low conductivity materials like ceramics. For the assisted electrode approach, the plasma channel radius calculations from the preceding section may estimate the maximum heat flow. Figure 4 and 8 determine the maximum heat flow for conductive materials, shown in Figure 17,18.

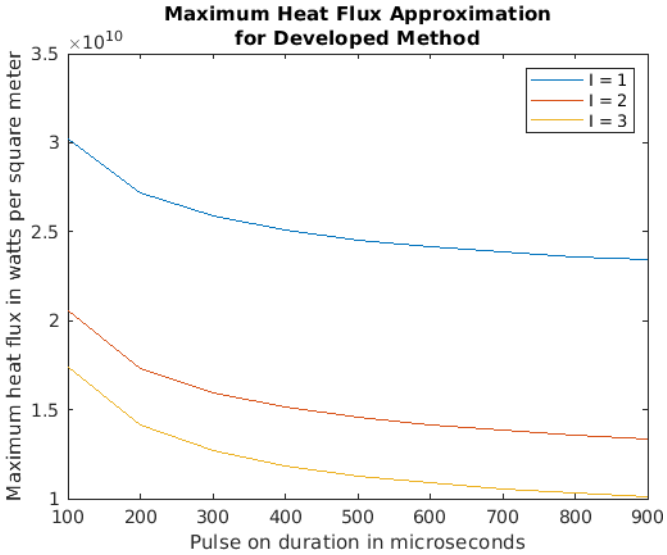

Figure 17: Maximum heat flux for the developed method at different peak current I (in amp) As pulse on time increases, peak current heat flow falls.

This is predicted as EDM heat propagates in a cylindrical coordinate and grows with time. Higher pulse-on time allows heat to disperse, reducing maximum heat flux. For a peak current, machining will smooth the surface at a greater pulse-on time. The highest heat flow may affect the thermal field surrounding the electrode and the machined surface roughness, even if the peak current requires the same energy input. Variations in pulse-on time may effect machining accuracy and cylindricity since rough machining lowers both. High peak current causes rougher surface. Lower current slows material removal but smooths the surface. The tests' machining output may be explained by this graph. Shorter pulse-on time for machining caused rough through-holes and reduced cylindricity.

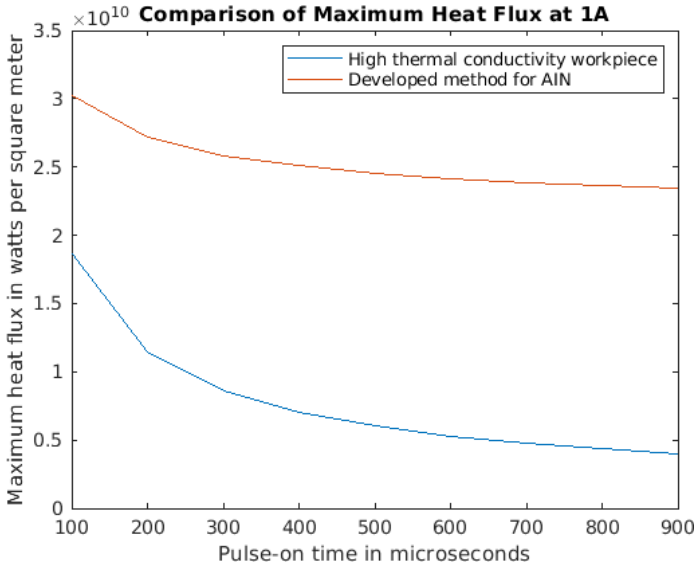

Figure 18: Comparison of maximum heat flux at 1A peak current

Another important finding is that peak current lowers maximum heat flux. Lower peak current increases electrode heat flux despite larger energy supply. Since material surrounding the electrode melted more easily, the aided electrode approach was able to create 1A peak current via holes.

Comparing maximum heat flux for conductive materials and the created approach in AIN ceramics shows that the proposed method has a greater maximum heat flux than traditional

methods. As thermal conductivity decreases, heat flow concentrates near the source. This is why melting and evaporation dominate material removal in the established approach. The surface gets rough and cracks and holes readily due to increased heat flux.

References

1. Alam, M. N., Siddiquee, A. N., Khan, Z. A., & Khan, N. Z. (2022). A comprehensive review on wire EDM performance evaluation. Proceedings of the Institution of Mechanical Engineers, Part E: Journal of Process Mechanical Engineering, 236(4), 1724-1746.
2. Blanco, D., Rubio, E. M., Lorente-Pedreille, R. M., & Saenz-Nuno, M. A. (2021). Sustainable processes in aluminium, magnesium, and titanium alloys applied to the transport sector: a review. Metals, 12(1), 9.
3. Chen, X. Wang, Z. Xu, J. Wang, Y. Li, J. and Liu, H. (2018). Sustainable production of micro gears combining micro reciprocated wire electrical discharge machining and precision forging, J. Clean. Prod., vol. 188, pp. 1–11, Jul. 2018, doi: 10.1016/j.jclepro.2018.03.200.
4. Dhir, R. K. Ghataora, G. S. and Lynn, C. J. (2017). 6 - Ceramic Applications, in Sustainable Construction Materials, R. K. Dhir, G. S. Ghataora, and C. J. Lynn, Eds. Woodhead Publishing, 2017, pp. 159–183.
5. Farooqui M. N. and Patil, N. G. (2018). A perspective on shaping of advanced ceramics by electro discharge machining, Procedia Manuf., vol. 20, pp. 65–72, Jan. 2018, doi: 10.1016/j.promfg.2018.02.009.
6. Gupta K., and N. K. Jain, (2014). Analysis and optimization of micro-geometry of miniature spur gears manufactured by wire electric discharge machining, Precis. Eng., vol. 38, no. 4, pp. 728–737, Oct. 2014, doi: 10.1016/j.precisioneng.2014.03.009.
7. Ho, K. H., Newman, S. T., Rahimifard, S., & Allen, R. D. (2004). State of the art in wire electrical discharge machining (WEDM). International Journal of Machine Tools and Manufacture, 44(12-13), 1247-1259.
8. Joshi S. N. and Pande, S. S. (2010). Thermo-physical modeling of die-sinking EDM process, J. Manuf. Process., vol. 12, no. 1, pp. 45–56, Jan. 2010, doi: 10.1016/j.jmapro.2010.02.001.
9. Joshi, S. N., & Pande, S. S. (2009). Development of an intelligent process model for EDM. The International Journal of Advanced Manufacturing Technology, 45, 300-317.
10. Kumar C. S. and Patel, S. K. (2018). Effect of WEDM surface texturing on Al2O3/TiCN composite ceramic tools in dry cutting of hardened steel, Ceram. Int., vol. 44, no. 2, pp. 2510–2523, Feb. 2018, doi: 10.1016/j.ceramint.2017.10.236.
11. Mohri, N. Fukuzawa, Y. Tani, T. Saito, N. and Furutani, K. (1996). Assisting Electrode Method for Machining Insulating Ceramics, CIRP Ann., vol. 45, no. 1, pp. 201–204, 1996, doi: 10.1016/S0007-8506(07)63047-9.
12. Rajeevalochanam P. and Ganesh Banda B. V., (2017). Mechanical Design and Analysis of Ceramic Stator Blades for Gas Turbine Stage, Mater. Today Proc., vol. 4, no. 8, pp. 8613–8623, 2017, doi: 10.1016/j.matpr.2017.07.209.
13. Sandu, A. V., Achitei, D. C., Perju, M. C., & Burduhos-Nergis, D. D. (2024). Perspective Chapter: Titanium–A Versatile Metal in Modern Applications. Titanium- Based Alloys-Characteristics and Applications: Characteristics and Applications, 3.
14. Thoe, T. B. Aspinwall, D. K. and Killey, N. (1999). Combined ultrasonic and electrical discharge machining of ceramic coated nickel alloy, J. Mater. Process. Technol., vol. 92–93, pp. 323–328, Aug. 1999, doi: 10.1016/S0924-0136(99)00117-X
15. Uhlmann E. and D. C. Domingos, (2016). Investigations on Vibration-assisted EDM-machining of Seal Slots in High-Temperature Resistant Materials for Turbine

Components –Part II, Procedia CIRP, vol. 42, pp. 334–339, Jan. 2016, doi: 10.1016/j.procir.2016.02.179.
16. Uhlmann E. and Domingos, D. C., (2013). Investigations on Vibration-Assisted EDM-Machining of Seal Slots in High-Temperature Resistant Materials for Turbine Components, Procedia CIRP, vol. 6, pp. 71–76, Jan. 2013, doi: 10.1016/j.procir.2013.03.019.
17. Xing, Y. Liu, L. Wu, Z. Wang, X. Huang, P. and Tang, L. (2018). Fabrication and characterization of micro-channels on Al2O3/TiC ceramic produced by nanosecond laser, Ceram. Int., vol. 44, no. 18, pp. 23035–23044, Dec. 2018, doi: 10.1016/j.ceramint.2018.09.106.
18. Zheng, Y., Zhang, K., Liu, T. T., W. H. Liao, C. D. Zhang, and H. Shao, (2019). Cracks of alumina ceramics by selective laser melting, Ceram. Int., vol. 45, no. 1, pp. 175– 184, Jan. 2019, doi: 10.1016/j.ceramint.2018.09.149.